Bioorg. Med. Chem. Lett. 43 (2021) 128058

Contents lists available at ScienceDirect

Bioorganic & Medicinal Chemistry Letters

journal homepage: www.elsevier.com/locate/bmcl

# Discovery of 2-amino-3-amido-5-aryl-pyridines as highly potent, orally bioavailable, and efficacious PERK kinase inhibitors

Veronica Calvo [a], David Surguladze [a], An-Hu Li [a], Matthew D. Surman [b], Srikanth Malibhatla [c], Madhavarao Bandaru [c], Suresh Krishna Jonnalagadda [c], Ravi Adarasandi [c], Madhusudhan Velmala [c], Durga Rama Prasad Singireddi [c], Mahendar Velpuri [c], Bhaskar Reddy Nareddy [c], Visweswara Sastry [c], Chiranjeevi Mandati [c], Rambabu Guguloth [c], Shapi Siddiqui [c], Basanagoud S. Patil [c], Elena Chad [d], Jennifer Wolfley [d], Jennifer Gasparek [d], Kirsten Feldman [d], Matthew Betzenhauser [d], Brent Wiens [d], Mary Koszelak-Rosenblum [d], Guangyu Zhu [d], Hongwen Du [e], Alan C. Rigby [a], Mark J. Mulvihill [a,*]

[a] HiberCell Inc. 619 West 54th Street, New York, NY 10019, USA
[b] AMRI, 26 Corporate Circle, Albany, NY 12203, USA
[c] AMRI, Plot #9, MN Park, Turkapally, Shameerpet, Genome Valley, RR District, Hyderabad 500078, India
[d] AMRI, 1001 Main Street, Buffalo, NY 14203, USA
[e] Pharmaron Beijing, Co. Ltd., No. 6, TaiHe Road, BDA, Beijing 100176, China

ARTICLE INFO

*Keywords:*
PERK
UPR
Kinase
Inhibitor
Orally bioavailable
786-O cell
Efficacy
Cancer
Structure–activity-relationships (SAR)

ABSTRACT

The protein kinase R (PKR)-like endoplasmic reticulum kinase (PERK) is one of the three endoplasmic reticulum (ER) transmembrane sensors of the unfolded protein response (UPR) that regulates protein synthesis, alleviates cellular ER stress and has been implicated in tumorigenesis and prolonged cancer cell survival. In this study, we report a series of 2-amino-3-amido-5-aryl-pyridines that we have identified as potent, selective, and orally bioavailable PERK inhibitors. Amongst the series studied herein, compound (**28**) a (*R*)-2-Amino-5-(4-(2-(3,5-difluorophenyl)-2-hydroxyacetamido)-2-ethylphenyl)-*N*-isopropylnicotinamide has demonstrated potent biochemical and cellular activity, robust pharmacokinetics and 70% oral bioavailability in mice. Given these data, this compound (**28**) was studied in the 786-O renal cell carcinoma xenograft model. We observed dose-dependent, statistically significant tumor growth inhibition, supporting the use of this tool compound in additional mechanistic studies.

It is well established that tumor cells are endowed with the ability to survive in a stressed, hostile microenvironment that is caused in part by nutrient and oxygen deprivation, high metabolic demand, and oxidative stress.[1] These and other established stressors are known to disrupt the protein folding capacity of the endoplasmic reticulum (ER), eliciting a robust cellular repair response known as the unfolded protein response (UPR).[2] Similarly, tumors utilize the UPR for survival under stressed conditions that are exacerbated by treatment with standard of care (SOC) therapeutic agents and chemotherapy.[3] The UPR enables cancer cell survival, supporting the tumorigenic potential of cancer cells, tumor metastasis, tumor drug resistance, all while enabling cancer cells to avoid effective immune detection and response.[4] Under extreme stress, the UPR switches the cellular machinery toward apoptosis.

The protein kinase R (PKR)-like endoplasmic reticulum kinase (PERK) is one of the three major ER transmembrane sensors of the UPR that regulates protein synthesis, aids cells to alleviate the impact of endoplasmic reticulum stress and has been implicated in tumorigenesis and cancer cell survival.[5] Activated PERK phosphorylates and activates its downstream substrate, eukaryotic initiation factor 2α (eIF2α), which inhibits the ribosome translation initiation complex to attenuate protein synthesis and decrease the amount of protein entering the ER. This adaptive, phenotypic mechanism allows cells to adapt and thus cope with ER stress,[6] by limiting misfolded protein accumulation, increasing ER-resident chaperone synthesis, enhancing protein clearance, and

* Corresponding author.
*E-mail address:* mmulvihill@hibercell.com (M.J. Mulvihill).

https://doi.org/10.1016/j.bmcl.2021.128058
Received 7 March 2021; Received in revised form 12 April 2021; Accepted 19 April 2021
Available online 23 April 2021
0960-894X/© 2021 The Author(s). Published by Elsevier Ltd. This is an open access article under the CC BY-NC-ND license (http://creativecommons.org/licenses/by-nc-nd/4.0/).

preventing the accumulation of additional misfolded proteins.[7–9]

Phosphorylation of eIF2α also increases translation of upstream open reading frame (uORF)-containing mRNAs including the transcription factor ATF4. ATF4 transcriptional targets include numerous genes involved in cellular adaptation and survival with roles in protein folding, nutrient uptake, amino acid metabolism, redox homeostasis, and autophagy. Selective and potent inhibition of the PERK arm of the UPR is expected to profoundly impact tumor cell fitness and survival in adverse 'stressed' conditions that are triggered following chemotherapy treatment and generally found within the tumor or metastatic niche.

Given the prevalence of stress biology mechanisms in cancer recurrence and metastatic disease, compounds that inhibit PERK represent a differentiated opportunity for the treatment of cancer.

Small molecule PERK inhibitors have been previously documented in the patent literature[10] as well as journal publications. Selected examples, including GSK2656157 (**1a**),[11] GSK2606414 (**1b**),[12] Compounds **2**–**4**,[13] and AMG-44 (**5**)[14] are shown in Fig. 1. Herein, we report the synthesis and discovery of a series of 2-amino-3-amido-5-arylpyrdines (**I** and **II**) that are highly potent, selective, and orally bioavailable PERK inhibitors capable of demonstrable efficacy in mouse xenograft tumor models.

We have leveraged literature reports for compound **4** to drive a medicinal chemistry effort that was iteratively supported by an X-ray crystallography structure-based approach to develop and refine structure–activity relationship (SAR) information. Collectively this approach permitted us to optimize the physiochemical and ADME/PK properties of this series. Different R, $R^1$, $R^2$, and L groups have been introduced into our PERK small molecule library to tune the potency and drug-like properties, such as aqueous solubility and permeability.

Compounds **I** were synthesized according to Scheme 1. 2-Amino-5-bromonicotinic acid reacted with amine **I-2** under classical amide coupling conditions to give bromo-amide **I-3**. A Pd-catalyzed Suzuki reaction between bromide **I-3** and boronate ***I*-4** afforded biaryl aniline **I-5**, which underwent amide coupling with acid **I-6** to generate the final product **I**.

When optimizing the R group in Compound **II**, the synthetic sequence illustrated in Scheme 2 was followed. Suzuki coupling between methyl 2-amino-5-bromonicotinate (**II-1**) and 3-methyl-4-(4,4,5,5-tetramethyl-1,3,2-dioxaborolan-2-yl)aniline (**II-2**) gave compound **II-3**. Coupling of aniline **II-3** with acid **II-4** generated amide **II-5**. The ester group in **II-5** was hydrolyzed into acid **II-6**, which was used to generate ester and amide products **II** in racemic forms by reacting with alcohol or amine **I-2** under coupling conditions. The racemic **II**'s were separated into pure enantiomers by chiral SFC.

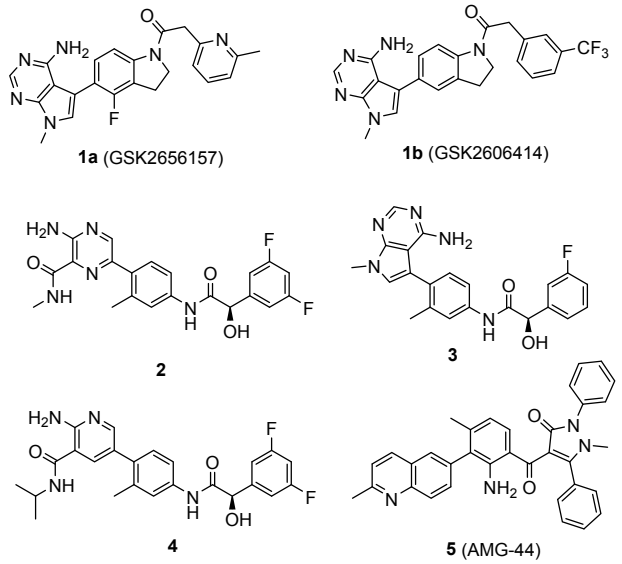


**Fig. 1.** Selected PERK inhibitors reported in the literature.

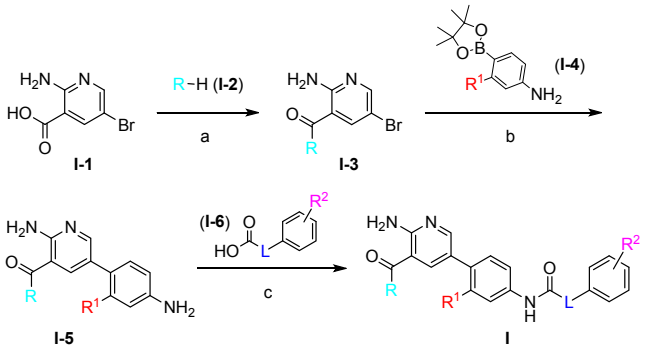


**Scheme 1.** General synthesis of PERK inhibitors (I): Reactions: a) EDC, HOBt, THF, 16 h; b) $PdCl_2(dppf)$, $K_2CO_3$, dioxane, $H_2O$, 90 °C, 16 h; c) HATU, DIPEA, THF, rt, 16 h.

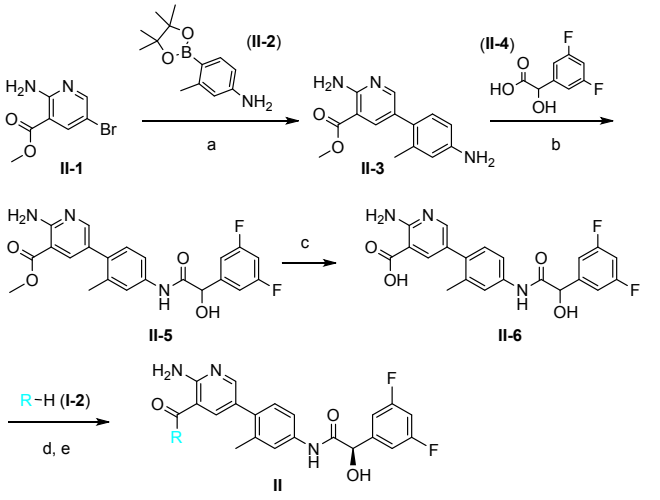


**Scheme 2.** General synthesis of PERK inhibitors (II): Reactions: a) $PdCl_2(dppf)$, $K_2CO_3$, dioxane, $H_2O$, 55 °C, 12 h; c) HATU, DIPEA, THF, rt; c) LioH, $H_2O$, MeOH·THF, d) HATU, DIPEA, THF; e) Chiral SFC separation.

In order to assess the potential of the compounds to specifically inhibit the PERK kinase pathway, compounds **I** and **II** were screened using two *in vitro* assays, (1) a PERK biochemical assay (which measures the direct effect of the compounds on the recombinant PERK protein to phosphorylate its direct target eIF2α)[14] and (2) a p-eIF2α cellular TR-FRET assay (to assess the ability of the compounds to cross the cell membrane and inhibit the direct phosphorylation of the substrate eIF2α). These data have been summarized in Table 1.

The following SAR trends were observed. For the L group substitutions, the OH was important for both biochemical and cellular activities. Removal of the OH group caused an 8-fold loss of PERK biochemical potency (**7** *vs.* **8**). Replacing the CH(OH) group with an O, NH, or $CH(NH_2)$ group or methylation of the OH group similarly diminished the potencies in all assays (**7** *vs.* **9**, **10**, **14**, and **11**).

We similarly observed within these L group substitutions that the (*R*)-chirality was preferred over (*S*)-chirality. The (*R*)-enantiomer **4** was 6-fold more potent than the (*S*)-enantiomer **6** against PERK. This trend translated to the p-eIF2α cellular assay and throughout the series.

The methyl substituted tertiary alcohol in L significantly decreased the PERK and p-eIF2α potencies (**12** *vs.* **7**), suggesting limited tolerance to steric bulk at that position.

On the terminal phenyl ring, lipophilic groups, such as halogen and small alkyls, were generally well tolerated (**4** and **22–24**).

**Table 1**
*In vitro* data of PERK inhibitors **4** and **6**–**29**.

| Compound No. | R | $R^1$ | L | $R^2$ | PERK $IC_{50}$ (μM) | p-eIF2α $IC_{50}$ (μM) |
|---|---|---|---|---|---|---|
| | 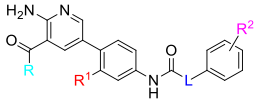 I and II | | | | | |
| **4** |  | Me |  | 3,5-di-F | 0.004 | 0.033 |
| **6** |  | Me |  | 3,5-di-F | 0.026 | 0.187 |
| **7** |  | Me |  | H | 0.009 | 0.198 |
| **8** |  | Me | $CH_2$ | H | 0.073 | 0.307 |
| **9** |  | Me | O | H | >1.00 | >10.0 |
| **10** |  | Me | NH | H | 1.35 | 2.36 |
| **11** |  | Me |  | H | >1.00 | 3.34 |
| **12** |  | Me |  | H | 0.130 | 2.13 |
| **13** |  | Me |  | H | 0.159 | 3.02 |
| **14** |  | Me |  | H | 1.46 | 3.27 |
| **15** | OH | Me |  | 3,5-di-F | 0.241 | N/D* |
| **16** |  | Me |  | 3,5-di-F | 0.019 | 0.049 |
| **17** |  | Me |  | 3,5-di-F | 0.015 | 0.058 |
| **18** |  | Me |  | 3,5-di-F | 0.599 | 2.22 |
| **19** |  | Me |  | 3,5-di-F | 0.004 | 0.045 |
| **20** |  | **Me** |  | **3,5-di-F** | **0.003** | **0.027** |
| **21** |  | Me |  | 3,5-di-F | 0.033 | 0.114 |
| **22** |  | Me |  | 3-Cl | 0.003 | 0.040 |
| **23** |  | Me |  | 3-Me | 0.003 | 0.054 |
| **24** |  | Me |  | 3-Et | 0.006 | 0.018 |
| **25** |  | H |  | 3,5-di-F | 0.023 | 0.313 |
| **26** |  | F |  | 3,5-di-F | 0.017 | 0.072 |
| **27** |  | Cl |  | 3,5-di-F | 0.009 | 0.023 |
| **28** |  | **Et** |  | **3,5-di-F** | **0.002** | **0.009** |
| **29** |  | OMe |  | 3,5-di-F | 0.085 | 0.366 |

* Not determined.

On the proximal phenyl ring, methyl, ethyl, or chloro substitution at the 2-position gave the best potencies in all assays tested (**4**, **27**, and **28**). The smaller hydrogen and fluoro groups at the same position decreased both biochemical and cellular potencies (**25**–**26** *vs.* **4**). The MeO substitution also significantly reduced *in vitro* potency (**29** *vs.* **4**). Replacement of the proximal phenyl ring with the 4-fluoroindolinyl moiety of compound **1a** afforded a significant (36x) loss in potency and solubility (compound **76**, Supporting Information) suggesting key pharmacophores from compound **1a** were not transferable to series **I** and **II** described herein.

At the 3-position on the pyridinyl ring, a secondary amido group was preferred. The tertiary amido ($CONMe_2$) substitution abolished both biochemical and cellular potencies (**18** *vs.* **17** and **4**). *N*-Methyl, ethyl, isopropyl, and cyclopropyl amido groups were generally well tolerated, while the *N-tert*-butyl amido appeared to cause some loss of both biochemical and cellular potencies (**21**). The acid group was not tolerated and caused loss of potency. Isopropyl ester (**16**) was active, although slightly less so when compared to its amido counterpart (**4**).

According to the above SAR observations, a combination of $R^1$ = methyl, L = (*R*)–CH(OH), and $R^2$ = 3,5-difluoro was preferred and selected for optimized biochemical and cellular potency.

We then examined the SAR for the 2-amino-3-amido-pyridin-3-yl region, while keeping the $R^1$ = methyl, L = (*R*)–CH(OH), and $R^2$ = 3,5-difluoro combination constant. The findings are listed in Table 2.

Replacing the pyridinyl ring with a pyrazinyl ring had a marginal effect on the potencies (**4** *vs.* **2** and **30**). However, unlike pyrazinyl, the pyridazinyl ring was not tolerated. The pyridazinyl analog caused drastic loss of both biochemical and cellular potencies (**4** *vs.* **31**). It appeared that the extra nitrogen disrupted the hinge binding of the 2-aminopyridinyl group.

A systematic investigation of various substituted pyridinyl groups provided additional SAR information: (1) The pyridin-3-yl without

**Table 2**
*In vitro* data of PERK inhibitors with different hinge binders (**2, 4, 30**–**37**).

| Cmpd | Ar = | PERK $IC_{50}$ (μM) | p-eIF2α $IC_{50}$ (μM) |
|---|---|---|---|
| |  III | | |
| **2** |  | 0.008 | 0.040 |
| **4** |  | 0.004 | 0.033 |
| **30** |  | 0.005 | 0.042 |
| **31** |  | >1.0 | 7.65 |
| **32** |  | 0.027 | 0.181 |
| **33** |  | 0.068 | 0.638 |
| **34** |  | 0.129 | 4.03 |
| **35** |  | 0.175 | >10.0 |
| **36** |  | >1.0 | >10.0 |
| **37** |  | 0.075 | 2.47 |

further substitution retained a certain level of biochemical activity, but caused substantial loss of cellular potency (**35**); (2) A 2-methyl substitution on the pyridin-3-yl caused further loss in both biochemical and cellular activities (**36**); (3) A 2-amino substitution (**37**) gained back activity in both assays tested compared to **35** and **36**, suggesting a potential bidentate binding with the hinge region of PERK; (4) The 3-amido group played an important role in maintaining the potencies. As long as the 3-amido substitution was retained, significant biochemical and cellular activities were preserved (albeit with reduced potency) even with possible disruption of hinge binding through the removal of the 2-amino group (**32**) or placement of a methyl group at the 2-position (**33**); (5) Methyl substitution on the 2-amino group markedly decreased both biochemical and cellular potencies (**4** *vs*. **34**), suggesting there is very limited space around the 2-amino position as well as a preferred intramolecular H-bonding interaction between the amino group and the amide carbonyl.

The hinge binder exploration identified 2-amino-3-amido-pyridinyl and 2-amino-3-amido-pyrazinyl as optimal groups that afforded potent PERK inhibitors.

To further elucidate the requisite direct binding interactions between PERK inhibitors **I** and **II** and the target while further informing our SAR approach through co-complex confirmational data, a crystallography screening effort was employed. Various compounds from the series were explored in co-crystallization studies with the PERK kinase. These efforts have resulted in a co-crystal structure of PERK bound to compound **20** (Fig. 2).

This co-crystal structure with compound **20** confirmed our hypothesized binding mode within the PERK kinase domain. Compound **20** is embedded in between the N- and C-terminal lobes of PERK with a packing surface area of 389 Å$^2$. The 2-amino-pyridinyl group forms bidentate hydrogen bonds with C891 in the hinge on the main chain. The (*R*)-enantiomer of the hydroxyl group also forms two additional hydrogen bonds with the side chain of D955 and main chain of F956. Given both D955 and F956 are located in the DFG motif of PERK, these hydroxyl mediated hydrogen bonds lock PERK into a DFG-D "in" conformation. The 3,5-difluorophenyl ring was further stabilized by hydrophobic packing from the side chains of a number of PERK residues, such as L643, L646, Y654, I886, and M888. Among these residues, L643 and L646 are located within the αC-helix. The binding of compound **20** caused this αC-helix to be displaced. Collectively, these interactions and the resultant conformational support that compound **20** is type 1.5 kinase inhibitor.[15] It should be noted that a water molecule might also contribute to compound **20**'s interactions, although no solvent molecule has been modeled into the structure in Fig. 2 due to the low occupancy and resolution.

Through the SAR exploration and optimization, several highly potent compounds, i.e., **19**, **20**, **22**, **27**, and **28**, were identified and further studied for their drug-like properties. These data are summarized in Table 3.

The aqueous solubility of this small set of compounds ranged from 10 to 48 μM and was deemed sufficient for *in vitro* and *in vivo* assessment. Compounds showed high permeability in the Caco-2 assay with efflux ratios ranging from 2 to 4.6.

This set of compounds was highly plasma-bound in all species tested, which is typical for many kinase inhibitors.

Regarding *in vitro* metabolic stability, we observed that the compounds were relatively stable in both human and dog hepatocytes and were characterized with long half-lives. However, we did notice that in rat hepatocytes, these compounds tended to be cleared rapidly except for compound **20**. Compound **28** demonstrated improved or comparable hepatocyte stability over reference compound **4** across the species.

Based on the culmination of *in vitro* results, compound **28** was chosen as a suitable candidate for further evaluation.

Selectivity is very important for kinase inhibitors as there are over 500 kinases in the human kinome. Inhibiting kinases beyond the target of interest not only causes off-target activity, but also potentially more toxicity. Compound **28** was screened in the DiscoverX's scanMAX$^{SM}$ panel of 468 human kinases.[16] These data are illustrated below in Fig. 3.

Compound **28** showed a very clean kinase selectivity profile with S (35), S(10), and S(1) selectivity scores of 0.007, 0, and 0, respectively at a concentration of 1 μM. To further illustrate the differentiated selectivity profile of compound **28** and put these data in perspective, Table 4 highlights key selectivity differences between compound **1a** (GSK-157) and compound **28** at a concentration of 10 μM (lower numbers are suggestive of stronger hits in the matrix). In addition to inhibiting PERK, GSK-157 is a potent binder/inhibitor to such kinases as ABL1 (F317I) non-phosphorylated, Aurora kinase B, KIT, PDGFR-β and RIPK1 as captured within this comparison. The potent RIPK1 activity of GSK-157 has been previously noted in the literature.[17]

To further evaluate our PERK inhibitors, *in vivo* PK studies were performed for compounds **4** and **28** in mice. The parameters are listed in Table 5.

In mice, compound **28** showed robust pharmacokinetics with $C_{max}$ of 3353 ng/mL, $AUC_{0\text{-last}}$ of 5153 h*ng/mL, and bioavailability of 70%, significantly improved over reference compound **4**.

High biochemical and cellular potencies, improved drug-like properties, excellent PK, and exceptional kinase selectivity make compound **28** a suitable candidate for efficacy studies in tumor models.

To assess the anti-tumor efficacy of compound **28** we have chosen the clear cell renal cell carcinoma (ccRCC) xenograft model 786-O. The 786-O model is driven by the Von Hippel-Lindau (VHL) mutation, which leads to PERK pathway activation.[18] Mice were implanted with ccRCC 786-O cells. Once the tumor reached 140–150 mm$^3$, mice were treated with vehicle or compound **28** at 3 mg/kg or 10 mg/kg BID for 28 days, and tumor growth inhibition (TGI) was measured. A BID dosing schedule was chosen based on the compound's PK profile with a $t_{1/2}$ of approximately 2 h. In this xenograft model, treatment with compound **28** led to a TGI of around 40% at 10 mg/kg BID and showed a dose

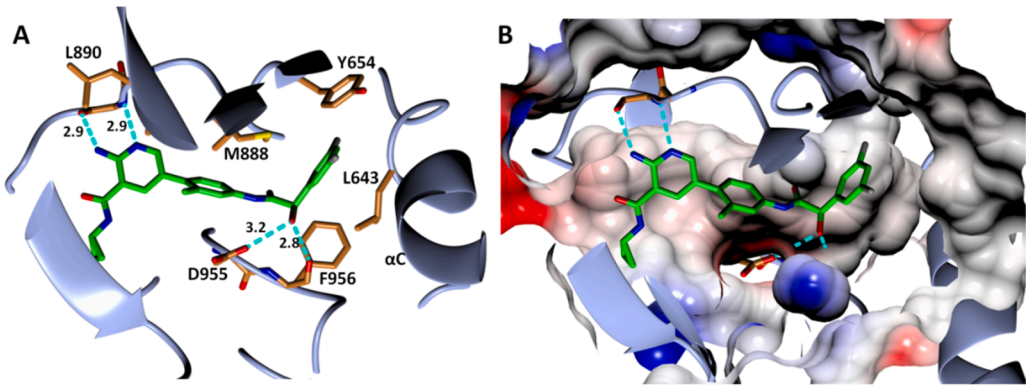


**Fig. 2.** Crystal structure of compound **20** bound to the PERK kinase domain. (a) View of inhibitor **20** in the PERK active site. The PERK backbone is rendered as a blue ribbon, while the side chains are illustrated in a cylindrical format with carbon atoms in brown, nitrogen atoms in blue, and oxygen atoms in red. Compound **20** is shown in cylinder format with the same color scheme with the exception that carbon atoms are now colored green. (b) View of inhibitor **20** in the PERK active site with molecular surface rendering. The color intensity corresponds to the calculated electrostatic potential, from −20 kT/e (red) to +20 kT/e (blue).

**Table 3**
Solubility, permeability, plasma protein binding and hepatocyte clearance properties of selected PERK inhibitors.

| Cmpd No. | Aqueous Solubility (μM) | Caco-2 | | Plasma Protein Binding | | | | Hepatocyte Clearance ($t_{1/2}$ min) | | | |
|---|---|---|---|---|---|---|---|---|---|---|---|
| | | $P_{app}$ (A → B) ($10^{-6}$ cm/s) | Efflux ratio | Human | Rat | Mouse | Dog | Human | Rat | Mouse | Dog |
| **4** | 31 | 15 | 2.0 | 99.3 ± 0.1 | 97.6 ± 0.1 | 98.3 ± 0.1 | 98.6 ± 0.1 | 245 | 9.3 | 69 | 187 |
| **19** | 48 | 14 | 3.3 | 98.1 ± 0.2 | 96.7 ± 0.5 | 97.2 ± 0.2 | 97.1 ± 0.3 | 118 | 34 | 69 | 877 |
| **20** | 37 | 14 | 4.6 | 97.6 ± 0.4 | 97.2 ± 0.3 | 97.1 ± 0.2 | 97.1 ± 0.4 | 474 | 131 | 48 | >1000 |
| **22** | 13 | 22 | 2.8 | 99.6 ± 0.1 | 98.7 ± 0.1 | 99.4 ± 0.1 | 99.4 ± 0.0 | 259 | 12 | 47 | 224 |
| **27** | 13 | 24 | 2.5 | 99.7 ± 0.1 | 99.3 ± 0.0 | 99.5 ± 0.0 | 99.5 ± 0.0 | 569 | 12 | 24 | 431 |
| **28** | 10 | 22 | 2.3 | 99.7 ± 0.1 | 99.3 ± 0.1 | 99.4 ± 0.1 | 99.8 ± 0.0 | 310 | 14 | 63 | 493 |

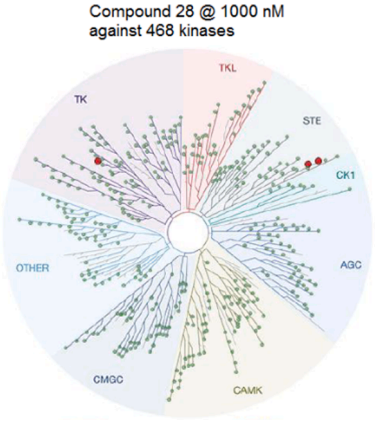


**Fig. 3.** The TREE*spot*™ interaction map of Compound **28** in the 468-kinase scanMAX℠ panel.

**Table 4**
KINOMEscan™ screening comparison of GSK-157 *vs* compound **28** at a concentration of 10 μM versus select kinases.

| % Control @ 10 μM Kinase | GSK-157 (**1a**) | Compound **28** |
|---|---|---|
| ABL1 (F317I) nonphos | 0.0 | 100 |
| AURKB | 5.3 | 75 |
| AXL | 8.2 | 70 |
| CSF1R | 1.8 | 74 |
| DDR1 | 1.3 | 100 |
| KIT | 0.1 | 67 |
| P38-γ | 3.7 | 87 |
| PDGFR-β | 0.2 | 60 |
| RIPK1 | 0.0 | 100 |
| SRC | 7.0 | 97 |
| TIE2 | 5.3 | 85 |
| TRKB | 6.5 | 100 |

Selectivity score @10uM: GSK-157 = 0.231; Compound **28** = 0.042.

**Table 5**
*In vivo* pharmacokinetics (PK) properties of selected PERK inhibitors.

| Compound | Mouse PK (10 mg/kg, PO) | | | |
|---|---|---|---|---|
| | $C_{max}$ (ng/mL) | $AUC_{0\text{-}last}$ (h*ng/mL) | $t_{1/2}$ (h) | F (%) |
| **4** | 1603 | 2005 | 1.2 | 49 |
| **28** | 3353 | 5153 | 2.0 | 70 |

response effect compared to the 3 mg/kg, BID dosing group (Fig. 4).

In conclusion, a series of 2-amino-3-amido-5-aryl-pyridines were discovered as highly potent PERK inhibitors. The reported compounds have demonstrable *in vitro* and *in vivo* activity with single-digit nanomolar biochemical and low- double-digit nanomolar cellular potencies, outstanding kinase selectivity, and have demonstrated favorable drug-like properties, robust pharmacokinetics, and oral bioavailability. Amongst the compounds studied, compound **28** has a favorable

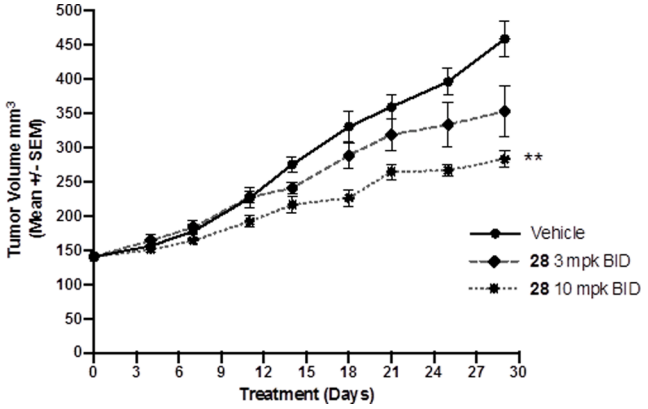


**Fig. 4.** *In vivo* anti-tumor activity of compound **28**. Mice bearing 786-O RCC xenograft tumors were treated twice daily (BID) with vehicle or compound **28** at 3 or 10 mg/kg. Treatments were started once tumors reached a volume of 140–150 $mm^3$. P by one-way ANOVA at day 28.

development candidate profile and was therefore selected for efficacy studies. In the 786-O renal cell carcinoma xenograft tumor model, compound **28** showed statistically significant tumor growth inhibition. Further optimization of this chemical series is currently in progress.

## Declaration of Competing Interest

The authors declare that they have no known competing financial interests or personal relationships that could have appeared to influence the work reported in this paper.

## Acknowledgments

We acknowledge the support of Advanced Photon Source beam line GMCA-CAT. GM/CA@APS has been funded in whole or in part with Federal funds from the NCI, National Institutes of Health, Grant ACB-12002 and NIGMS, National Institutes of Health, Grant AGM-12006. This research used resources of the Advanced Photon Source, a United States Department of Energy (DOE) Office of Science User Facility operated for the DOE Office of Science by Argonne National Laboratory under Contract DE-AC02-06CH11357.

## Appendix A. Supplementary data

Supplementary data to this article can be found online at https://doi.org/10.1016/j.bmcl.2021.128058.

## References

1 Walter P, Ron D. The unfolded protein response: from stress pathway to homeostatic regulation. *Science*. 2011;334:1081–1086. https://doi.org/10.1126/science.1209038.
2 Hetz C, Papa FR. The unfolded protein response and cell fate control. *Mol Cell*. 2018; 69:169–181. https://doi.org/10.1016/j.molcel.2017.06.017.

3 Urra H, Dufey E, Avril T, Chevet E, Hetz C. Endoplasmic reticulum stress and the hallmarks of cancer. *Trends Cancer*. 2016;2:252–262. https://doi.org/10.1126/science.1209038.

4 Bhat TA, Chaudhary AK, Kumar S, et al. Endoplasmic reticulum-mediated unfolded protein response and mitochondrial apoptosis in cancer. *Biochim Biophys Acta*. 2017;1867:58–66. https://doi.org/10.1016/j.bbcan.2016.12.002.

5 Harding HP, Zhang Y, Ron D. Protein translation and folding are coupled by an endoplasmic-reticulum-resident kinase. *Nature*. 1999;397:271–274. https://doi.org/10.1038/16729.

6 Shi Y, Vattem KM, Sood R, et al. Identification and characterization of pancreatic eukaryotic initiation factor 2 alpha-subunit kinase, PEK, involved in translational control. *Mol Cell Biol*. 1998;18:7499–7509. https://doi.org/10.1128/mcb.18.12.7499.

7 Urra H, Dufey E, Lisbona F, Rojas-Rivera D, Hetz C. When ER stress reaches a dead end. *Biochim Biophys Acta*. 2013;1833(12):3507–3517.

8 Marciniak SJ, Garcia-Bonilla L, Hu J, Harding HP, Ron D. Activation-dependent substrate recruitment by the eukaryotic translation initiation factor 2 kinase PERK. *J Cell Biol*. 2006;172:201–209. https://doi.org/10.1083/jcb.200508099.

9 Ron D, Walter P. Signal integration in the endoplasmic reticulum unfolded protein response. *Nat Rev Mol Cell Bio*. 2007;8:519–529. https://doi.org/10.1038/nrm2199.

10 Axten JM. Protein kinase R(PKR)-like endoplasmic reticulum kinase (PERK) inhibitors: a patent review (2010–2015). *Expert Opin Ther Pat*. 2017;27:37–48. https://doi.org/10.1080/13543776.2017.1238072.

11 Axten JM, Romeril SP, Shu A, et al. Discovery of GSK2656157: an optimized PERK inhibitor selected for preclinical development. *ACS Med Chem Lett*. 2013;4:964–968. https://doi.org/10.1021/ml400228e.

12 Axten JM, Medina JR, Feng Y, et al. Discovery of 7-methyl-5-(1-{[3-(trifluoromethyl)phenyl]acetyl}-2,3-dihydro-1H-indol-5-yl)-7H-pyrrolo[2,3-d]pyrimidin-4-amine (GSK2606414), a potent and selective first-in-class inhibitor of protein kinase R (PKR)-like endoplasmic reticulum kinase (PERK). *J Med Chem*. 2012;55:7193–7207. https://doi.org/10.1021/jm300713s.

13 (a) Cifuentes-Garcia, MM, Garcia-Paredes, MC. Phenyl-2-hydroxy-acetylamino-2-methyl-phenyl compounds. WO 2018/194885A1. (b) Mulvihill, MJ, Li, AH, Surman, MD. PERK inhibiting compounds. WO2021/041973A1.

14 Smith AL, Andrews KL, Beckmann H, et al. Discovery of 1H-pyrazol-3(2H)-ones as potent and selective inhibitors of protein kinase R-like endoplasmic reticulum kinase (PERK). *J Med Chem*. 2015;58:1426–1441. https://doi.org/10.1021/jm5017494.

15 Roskoski R. Classification of small molecule protein kinase inhibitors based upon the structures of their drug-enzyme complexes. *Pharmacol Res*. 2016;103:26–48. https://doi.org/10.1016/j.phrs.2015.10.021.

16 scanMaxSM Kinase Assay Panel. https://www.discoverx.com/services/drug-discovery-development-services/kinase-profiling/kinomescan/scanmax. Accessed 4 March, 2021.

17 Rojas-Rivera D, Delvaeye T, Roelandt R, et al. When PERK inhibitors turn out to be new potent RIPK1 inhibitors: critical issues on the specificity and use of GSK2606414 and GSK2656157. *Cell Death Differ*. 2017;24:1100–1110. https://doi.org/10.1038/cdd.2017.58.

18 Kuo, CY, Lin, CH, Hsu, T. VHL inactivation in precancerous kidney cells induces an inflammatory response via ER stress-activated IRE1α signaling. Cancer Res. 2017;77(13):3406-3416. doi: 10.1158/0008-5472.CAN-16-3196.